

INVITED REVIEWS

Solar flares: radio and X-ray signatures of magnetic reconnection processes

Marian Karlický

Astronomical Institute, Academy of Sciences of the Czech Republic, 251 65 Ondřejov, Czech Republic; karlicky@asu.cas.cz

Received 2013 December 20; accepted 2014 March 17

Abstract This review summarizes new trends in studies of magnetic reconnection in solar flares. It is shown that plasmoids play a very important role in this primary flare process. Using the results of magnetohydrodynamic and particle-in-cell simulations, we describe how the plasmoids are formed, how they move and interact, and how a flare current sheet is fragmented into a cascade of plasmoids. Furthermore, it is shown that during the interactions of these plasmoids electrons are not only very efficiently accelerated and heated, but electromagnetic (radio) emission is also produced. We also describe possible mechanisms for the triggering of magnetic reconnection. The relevant X-ray and radio signatures of these processes (such as radio drifting pulsation structures, narrowband dm-spikes, and the loop-top and above-the-loop-top X-ray sources) are then described. It is shown that plasmoids can also be formed in kinked magnetic ropes. A mapping of X-points of the magnetic reconnection on the chromosphere (as e.g. a splitting of flare ribbons) is mentioned. Supporting EUV and white-light observations of plasmoids are added. The significance of all these processes for the fast magnetic reconnection and electron acceleration is outlined. Their role in fusion experiments is briefly mentioned.

Key words: Sun: flares — Sun: radio radiation — Sun: X-rays

1 INTRODUCTION

Solar flares are explosive phenomena in the solar atmosphere, in which the energy accumulated in the magnetic field and electric currents is rapidly transformed into plasma heating, plasma flows, accelerated particles and emission in a broad range of electromagnetic waves: from radio, through optical, ultraviolet (UV), X-rays to gamma-rays. Solar flares are the most powerful magnetic events in the solar system, releasing an energy of up to 10^{32} erg in tens of minutes. The strongest flares are intimately associated with coronal mass ejections and with the acceleration of particles into interplanetary space. Observational aspects of solar flares have been summarized in several reviews, for example in Priest & Forbes (2002), Aschwanden (2002), Krucker et al. (2008), Schrijver (2009) and Fletcher et al. (2011).

There are several types of classifications of solar flares. Generally, flares can be divided into long duration event (LDE) flares and impulsive flares. In UV and extreme-ultraviolet (EUV) observational bands, the former have a cusp-shaped loop structure, but the latter do not and instead only have a

simple loop structure. Because these two types of flares differ, various models have been proposed to explain them. While the LDE flares are usually described by the “standard” CSHKP flare model (Carmichael 1964; Sturrock 1966; Hirayama 1974; Kopp & Pneuman 1976), impulsive flares are explained by the loop flare model, in which the energy release occurs inside the loop (Spicer 1977).

A scenario for the CSHKP model is as follows. First, along the neutral line between magnetic polarities in the active region, a magnetic rope (i.e. current-carrying loop) is formed due to shear and vortex plasma flows at the photospheric level. At its bottom part, cold, dense plasma condenses into the filament, which is dark, in contrast to the surrounding bright chromosphere. Then, this magnetic rope together with the filament becomes unstable due to internal instabilities or external perturbations (waves, shocks or particle beams). Another possibility is that the upper part of the magnetic rope interacts with the above-lying magnetic field lines and through magnetic reconnection a stabilizing magnetic force decreases (this is the breakout model; see, for example, Aurass et al. 2011). As a result the magnetic rope moves upwards, but its ends are still anchored in dense layers of the solar atmosphere, thus forming a growing current-carrying loop. Although an enormous electric current flows through this magnetic rope (up to 10^{12} A), this current does not dissipate here because the electric current density is low. The situation is different below the rising rope, where the current sheet is formed step by step. It is assumed that when this current sheet becomes sufficiently narrow and the current density inside this sheet is sufficiently high, then the magnetic reconnection sets in. A plasma together with magnetic field lines is pulled from both sides of the current sheet into the X-point region and accelerated to the Alfvén speed in vertical plasma outflows. The upward oriented outflow even accelerates the rising magnetic rope, while the downward oriented outflow is stopped above the flare loop arcade, where the so called termination shock can be generated. At the X-point within the magnetic reconnection region a strong electric field is generated, which accelerates electrons and ions to high energies. (For more details about particle acceleration, see the review by Zharkova et al. 2011.) These particles propagate along the magnetic field lines. Some of them propagate upwards in the solar atmosphere, generating radio emission by the plasma emission mechanism, such as type III radio bursts (Meshalkina et al. 2012). The electrons propagating downwards generate radio continua (at frequencies above ~ 2 GHz) by the gyro-synchrotron mechanism and the hard X-ray emission by bremsstrahlung (e.g. Kundu et al. 2009). Simultaneously, the electrons in the whole flare generate various fine structures in the radio spectrum via the plasma emission mechanisms (Bárta & Karlický 2005; Yan et al. 2010; Tan 2013). The superthermal ions, especially protons, propagating downwards are sources of gamma-rays (Vilmer et al. 2011). During the magnetic reconnection process the flare plasma is strongly heated, which leads to an increase in the soft X-ray emission. The whole magnetic flare structure expands and magnetohydrodynamic (MHD) shocks are produced (Dryer et al. 1998; Wang & Yan 2012). Such shocks then generate type II radio bursts. Furthermore, associated waves propagate along the solar surface as EIT (UV) and Moreton ($H\alpha$) waves (Thompson et al. 1999; Kumar et al. 2013). During some flares, even large amplitude kink oscillations (Nistico et al. 2013) and sunquakes (Zharkov et al. 2013) have been detected.

While this CSHKP model describes the global behavior of the LDE flares very well, detailed observations of the same flares show short-duration and spatially localized fragmented energy releases in, for example, clouds of the narrowband dm-spikes (Benz 1986). This duality in global and detailed observations is also expressed in the duality of flare models. Besides the CSHKP model, there is an alternative model that has many stochastically generated current sheets in a turbulent flare loop (Galsgaard & Nordlund 1996; Vlahos et al. 2004). An advantage of this alternative model is the occurrence of many reconnection X-points where particles are accelerated, which solves the problem of the amount of accelerated particles. Another problem with the CSHKP model is that, at the very beginning of formation of the current sheet below the rising magnetic rope, the width of the current sheet is comparable to the small radius of the magnetic rope (around a thousand kilometers). In such a broad current sheet, the current densities are too low for an effective dissipation. Therefore,

in agreement with Shibata & Tanuma (2001), a mechanism that makes the current sheet narrower and increases the current densities in this current sheet is needed.

This review paper presents new trends which try to solve the above mentioned problems. In addition, observations supporting these new ideas are added.

The paper is organized as follows. After the introduction we describe a model of fragmented reconnection in Section 2. Section 3 summarizes results of some recent numerical simulations of magnetic reconnection. In Section 4 we present observations supporting the model of the fragmented magnetic reconnection with plasmoids and a cascade of plasmoids. This paper ends with conclusions and remarks concerning plasma fusion experiments.

2 MODEL OF FRAGMENTED MAGNETIC RECONNECTION

This model not only tries to include a concept of multiple current sheets and X-points into the standard CSHKP flare model, but also fits observations better than any previous model. Let us start from the radio spectrum observed during the 2001 April 12 flare (Fig. 1). Besides quite common radio continua at high frequencies (above 2 GHz) generated by the gyro-synchrotron emission mechanism, and type III and II bursts at frequencies below 0.6 GHz generated by electron beams and the flare shock, at 10:17:20 – 10:22:00 UT in the 0.45–1.5 GHz range the drifting pulsation structure (DPS) was observed. As shown in the following, this narrowband and drifting burst is radio emission generated by the plasma emission mechanism by superthermal electrons that are trapped in a plasmoid. Compare this radio spectrum with the scheme showing the magnetic rope and plasmoids in Figure 1 (right).

The importance of plasmoids in magnetic reconnection in solar flares was recognized for the first time by Ohya & Shibata (1998), who studied an ejection of the plasmoid, observed during the 1992 October 5 flare in X-rays by *Yohkoh*. The same flare was also studied by Kliem et al. (2000) and it was shown that this plasmoid was associated with DPSs (see fig. 1 in Kliem et al. 2000). Similar observations, but made with the Nancay radioheliograph which delivers spatially resolved radio sources, were described by Khan et al. (2002). A model for this radio emission was proposed and further developed in papers by Karlický et al. (2002), Karlický (2004), Karlický & Bárta (2007), Bárta et al. (2008a) and Karlický et al. (2010). This model assumes that the vertical current sheet forms below the rising magnetic rope (Fig. 1 right). In the current sheet, the plasmoids (in 3-D the magnetic ropes) are formed due to tearing and merging (coalescence) processes, and particles (especially electrons) are very efficiently accelerated (Drake et al. 2005, 2006; Hoshino 2005; Pritchett 2006; Pritchett 2008; Karlický 2008). Most of the electrons are then trapped inside the plasmoids (in semi-closed magnetic field structures – an O-type structure in a 2-D magnetic field), where they generate Langmuir waves that produce DPSs through a wave transformation to electromagnetic waves. The DPS is generated in a limited range of frequencies due to the limited range of plasma densities (plasma frequencies) inside the plasmoid. Depending on the magnetic field structure in the flaring atmosphere, the plasmoids move upwards or downwards or even stay at the same height in the flaring atmosphere (Bárta et al. 2008a,b). Due to a preference of divergent magnetic field lines in the upward direction, most of the plasmoids move upwards and the corresponding DPSs drift towards lower frequencies. In some cases the plasmoids move downwards and interact with the underlying flare arcade, see Kolomanski & Karlický (2007) and Milligan et al. (2010).

All these processes can be considered as a fragmentation of the flare current sheet during the magnetic field reconnection. Two types of fragmentation were suggested: (a) fragmentation due to a stretching of the current sheet and the tearing-mode instabilities in a progressively narrower current sheet (cascading reconnection) (Shibata & Tanuma 2001), and (b) fragmentation between two merging plasmoids in generated current sheets on progressively smaller spatial scales (Bárta et al. 2010, 2011a,b; Karlický et al. 2012; and Ugai 2013). This concept was theoretically developed by Loureiro et al. (2007) and Uzdensky et al. (2010) as the theory describing chain plasmoid instability.

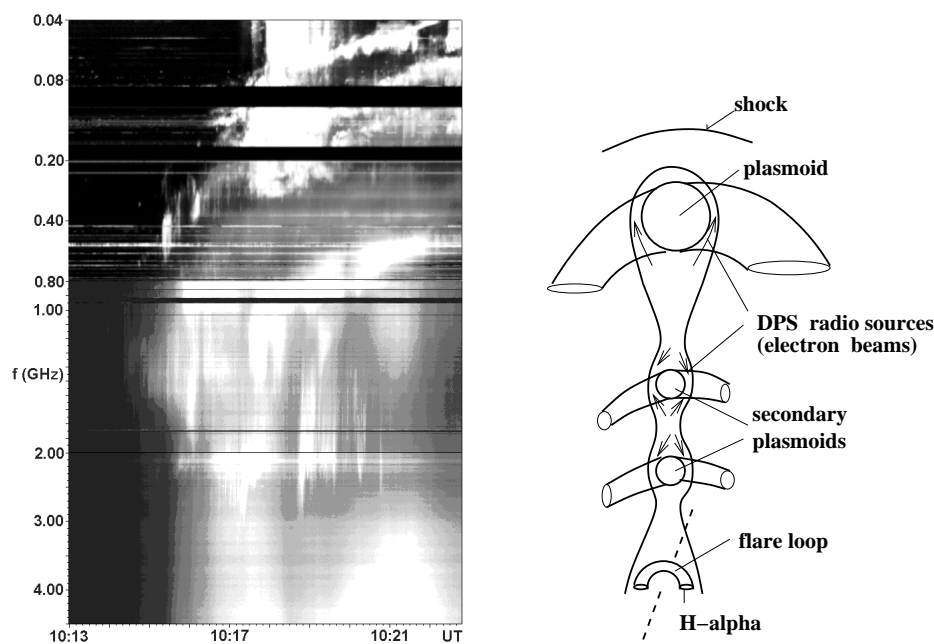


Fig. 1 *Left:* The 0.04–4.5 GHz radio spectrum observed during the 2001 April 12 flare by the Potsdam (0.04–0.8 GHz range) and the Ondřejov radiospectrographs (0.8–4.5 GHz), showing the DPS at 10:17:20 – 10:22:00 UT in the 0.45–1.5 GHz range and the type II radio burst (generated by a shock wave) at 10:17 – 10:33 UT in the 0.04–0.3 GHz range. *Right:* Flare scenario: The rising magnetic rope (the uppermost plasmoid) generates a vertical current sheet underneath, where further plasmoids (producing DPSs) are generated due to the tearing-mode instability. Above this main rope, the shock, producing a type II radio burst, is generated; compare this scenario with the radio spectrum in the left part of the figure.

Multi-scale magnetic islands were observed in the Earth's magnetotail (Hoshino et al. 1994) as well as in solar flares (Karlický 2004). An advantage of this concept is that it explains the generation of very narrow current sheets with high current densities, which are required for the anomalous resistivity generation and fast reconnection. Moreover, many magnetic X-points in this model provide sufficiently large volume for the acceleration of particles. Remark: Besides these fragmentations during the magnetic reconnection process, the current sheet can be fragmented due to shear plasma flows even before the magnetic reconnection event takes place, as shown recently by Nickeler et al. (2013).

3 MAGNETOHYDRODYNAMIC AND PARTICLE-IN-CELL SIMULATIONS OF MAGNETIC RECONNECTION PROCESSES

3.1 Initiation of Magnetic Reconnection

It is known that sometimes after a flare has occurred at some location, flares at distant locations also appear. These so called sympathetic flares (Fritzova-Švestková et al. 1976) indicate that there are some agents generated by the first flare that trigger these distant flares.

The first ideas about the triggering of flares appeared in the paper by Norman & Smith (1978). They argued that flares cannot start immediately in the whole flare volume and proposed that flares

are triggered in a very localized region and then flare processes spatially spread through the so called dissipative spreading process into the whole flare volume. They considered two types of agents spreading this dissipation: (a) electron beams or (b) shock waves. Thus, the same agents can be considered for the triggering of distant (sympathetic) flares or for an explanation of the so called domino effect in successive flares in one active region (Zuccarello et al. 2011). The effects of both proposed agents (beams or shocks) on magnetic reconnection were studied in papers by Karlický & Jungwirth (1989) and Odstrčil & Karlický (1997).

In the first paper, Karlický & Jungwirth (1989) assumed that the electron beam penetrates into the current-carrying system of the magnetic reconnection region and generates the Langmuir waves there. Then, using a particle-in-cell (PIC) model they studied how these electrostatic waves affect such a plasma system. They found that sufficiently strong Langmuir waves produce the ion-sound waves through the three-wave decay process (Bárta & Karlický 2000). These ion-sound waves increase the electrical resistivity at this electric current system and dissipative processes can start. Thus, they concluded that the electron beam can trigger magnetic reconnection.

On the other hand, the triggering process by shock waves was studied by Odstrčil & Karlický (1997). They used a 2-D MHD model and in the initial state they generated an MHD shock wave which propagated towards the current sheet. Some part of the shock wave went through the current sheet and the remaining part was reflected. At the very beginning of this shock-current-sheet interaction nothing happened. However, after some time a very specific plasma flow pattern around the current sheet was formed, which in the following times triggered magnetic reconnection in this current sheet. This shows that for magnetic reconnection there is not only an enhanced electric resistivity, but the plasma flows are also important for the triggering of magnetic reconnection. It is interesting that the same process was considered by Tanuma et al. (2001) for the triggering of the reconnection in the galactic current sheet. The only difference was that, instead of the flare, a supernova was considered as the source of the shock wave.

Besides these triggering agents (beams or shocks), the MHD waves were suggested as a trigger of magnetic reconnection. Nakariakov et al. (2006) proposed that the amplitudes of these waves are strongly amplified near the X-points and thus trigger magnetic reconnection. Furthermore, Sych et al. (2009) studied the amplitudes of the slow MHD waves, which propagated from a sunspot to its vicinity. They found that when the amplitude was at a maximum, these waves triggered flares near this sunspot. Recently, it was also shown that the current density inside the current sheet can be enhanced by shear flows (Nickeler & Wiegmann 2012).

3.2 Fragmented Reconnection

Bárta et al. (2011a) followed the idea of Shibata & Tanuma (2001) that the current sheet is fragmented due to the stretching tearing-mode instability and made appropriate numerical simulations. These simulations not only confirmed Shibata & Tanuma's idea but they also revealed an additional type of fragmentation; namely, fragmentation of plasmoids during plasmoid merging processes. A similar fragmentation process was also found in PIC simulations (Karlický et al. 2012).

An extensive study of the formation, motion and merging of plasmoids during magnetic reconnection was performed by Bárta et al. (2008b). Using MHD simulations, they studied cases with upwards and downwards moving plasmoids in the vertical current sheet in a gravitationally stratified atmosphere (Fig. 2 upper and middle rows). They found that the upwards or downwards motion of the plasmoid depends on the divergence or convergence of the surrounding magnetic field lines. At higher heights of the solar atmosphere the magnetic field lines are divergent in the upward direction; therefore, the plasmoids predominantly move upwards in the solar atmosphere. Furthermore, several plasmoids can be formed in the current sheet, which then interact and merge into a larger plasmoid, see Figure 2 bottom row. This merging process is sometimes followed by an oscillation of the resulting plasmoid (e.g. Karlický & Kliem 2010).

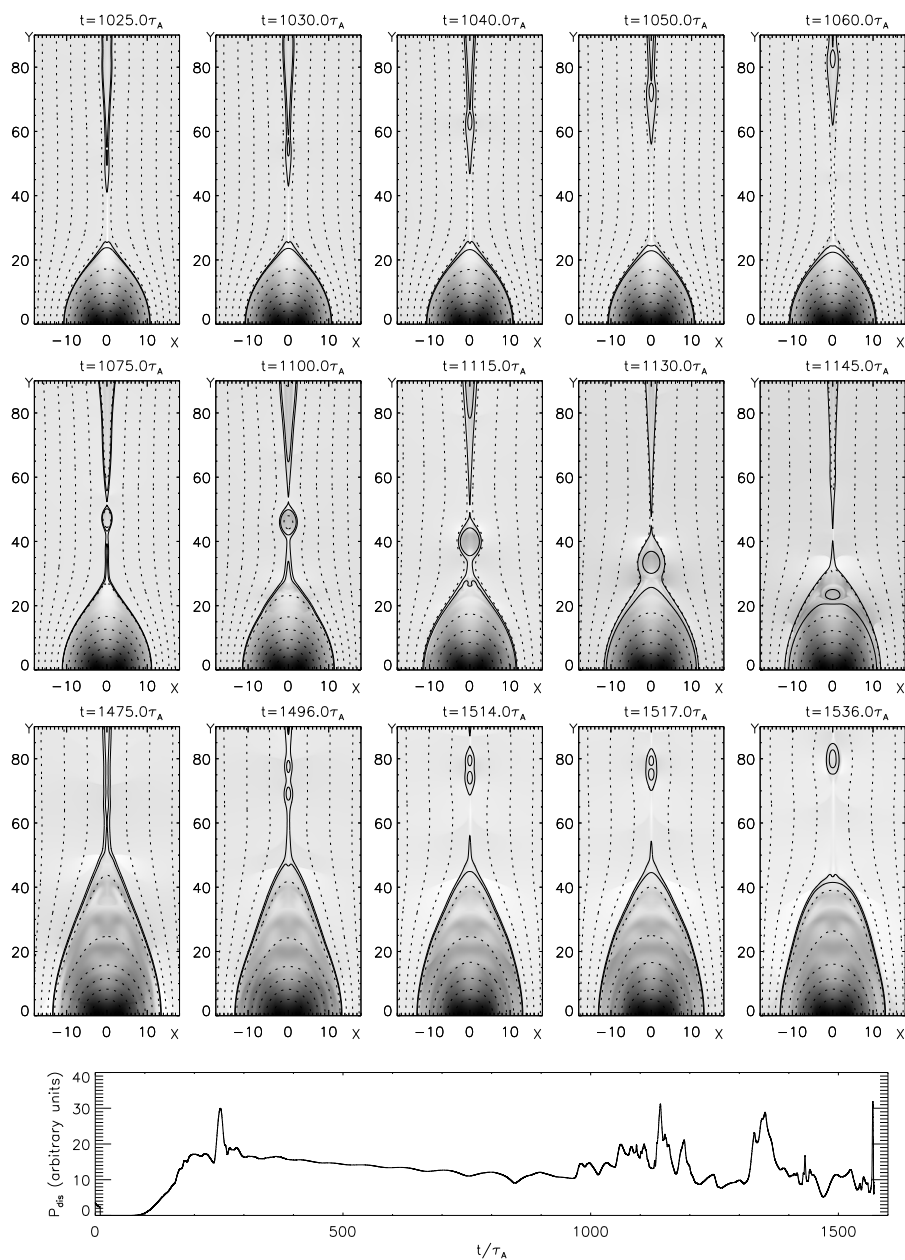


Fig. 2 The horizontal rows show upward-moving and downward-moving plasmoids resulting from MHD numerical simulations of the reconnection, tearing and coalescence processes in the vertical current sheet. *Bottom:* Time evolution of the power released in the reconnection.

A similar study of these processes was made by Karlický & Bárta (2011), but using a 2.5-D PIC model. The numerical range of the simulation was $L_x \times L_y = 600 \Delta \times 4000 \Delta$, where Δ ($=1$) represents the stepsize of the grid. In the initial state, the Harris current sheet was formed along the line $x = 0 \Delta$ and its half-width was $L = 10 \Delta$. The electron-proton plasma with the proton-electron

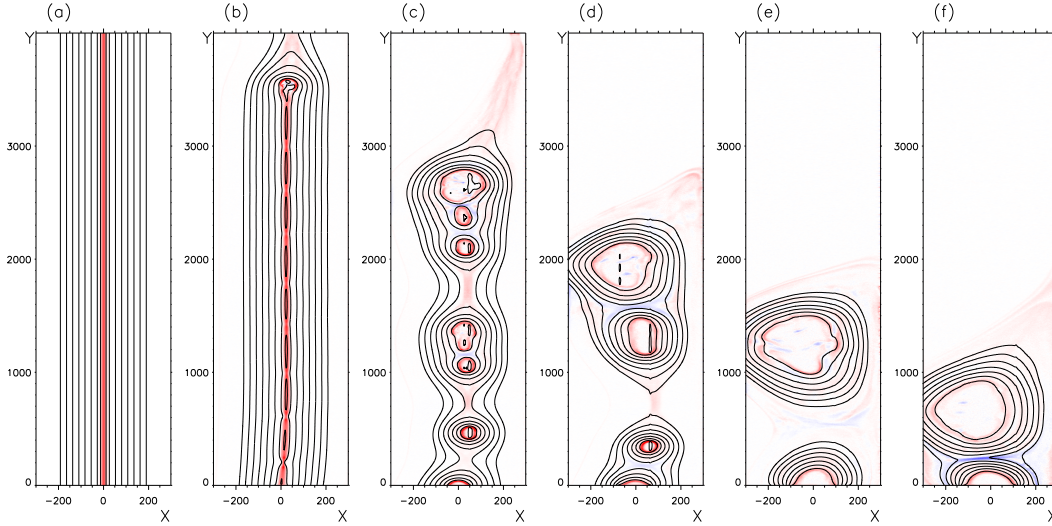


Fig. 3 Magnetic field lines and corresponding current densities (*red areas; color online*), obtained by the PIC simulations, in the x - y computational plane at six different times: at the initial state (a), at $\omega_{pe}t = 1800$ (b), at $\omega_{pe}t = 3500$ (c), at $\omega_{pe}t = 5000$ (d), at $\omega_{pe}t = 6500$ (e) and at $\omega_{pe}t = 8000$ (f).

mass ratio $m_p/m_e = 16$ was considered. This ratio is unrealistic but taken here to shorten the computations. Nevertheless, the electron mass is low enough to separate the dynamics of electrons and protons well. In each numerical cell located far from the current sheet, the authors initiated $n_0 = 60$ electrons and $n_0 = 60$ protons. In the current sheet, the initial number density was enhanced just to maintain an equilibrium in pressure. The initial electron temperature was set to $T = 10$ MK and regarded as the same in the whole numerical box, and the temperature of the protons was chosen to be the same as that for electrons. The plasma frequency was $\omega_{pe}\Delta t = 0.05$ (Δt is the timestep which equals 1), the electron Debye length was $\lambda_D = 0.6 \Delta$, and the electron and proton inertial lengths were $d_e = 10 \Delta$ and $d_i = 40 \Delta$, respectively. To study successive coalescence processes among several plasmoids, the authors initiated 10 plasmoids along the current sheet by a cosine perturbation of the electric current density in the sheet; with the k -vector $k = 2\pi \times 10/4000 = 0.0157 \Delta^{-1}$ and the amplitude corresponding to the current density \mathbf{j} given by the magnetic field in the current sheet ($\mathbf{j} = \nabla \times \mathbf{B}$). The plasma β parameter was taken as $\beta = 0.07$. Free boundary conditions as in the TRISTAN code (Matsumoto & Omura 1993) were used (i.e. the radiation-absorbing boundaries for fields, half of the particles escape and the remaining particles are reflected at the boundaries).

After initiation, the system evolved freely and plasmoids started to merge into larger and larger plasmoids (Fig. 3). During this merging process the electrons were very efficiently accelerated and heated. One of these acceleration regions was located at the X-point between these merging plasmoids. Most of these accelerated electrons were then trapped in the plasmoids, see the numerical electrons with energy above 40 keV (dots) in Figure 4. The white plus marks the location of the maximum plasma temperature (118.7 MK) in the system. Note that by using an unrealistically large electron-to-ion mass ratio the temporal scales are compressed. However, the main features of these fragmentation and acceleration processes remain realistic.

Using the same PIC model, Karlický et al. (2012) discovered that additional plasmoids were generated between two merging plasmoids (Fig. 5). This confirmed the idea that the current sheet is also fragmented during the merger of plasmoids and, thus, a cascade of plasmoids on smaller

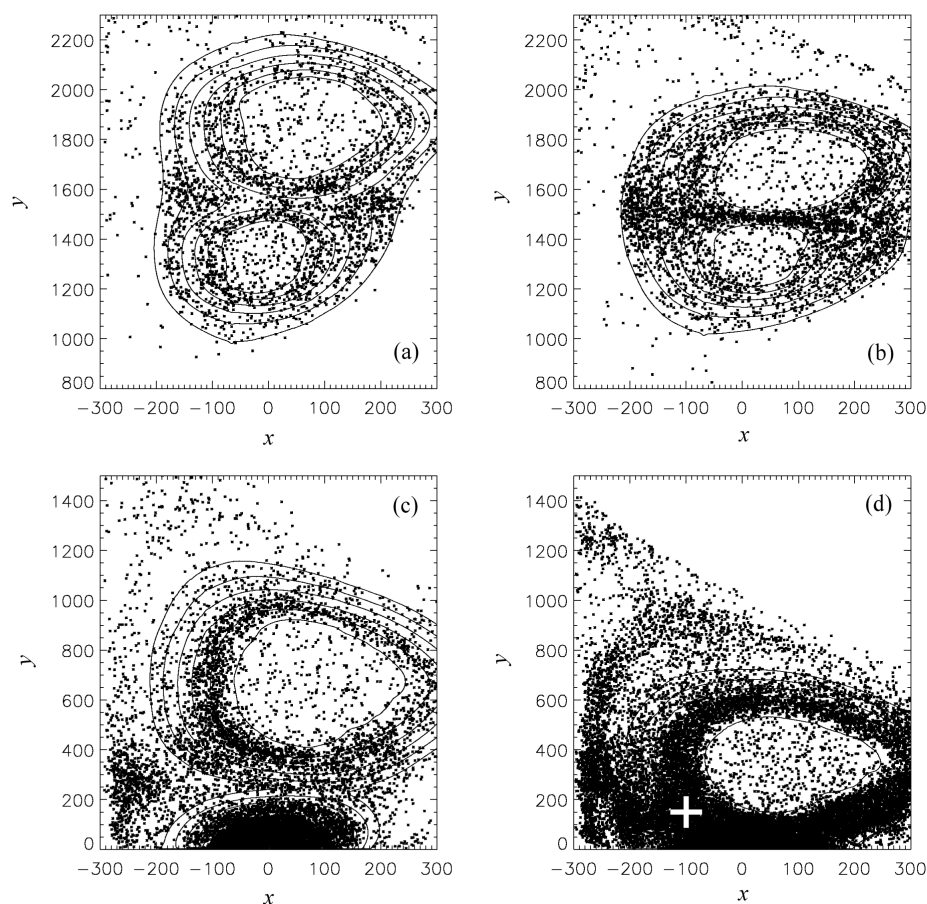


Fig. 4 PIC simulations: A detailed view of magnetic field lines in the x - y computational plane and distribution of numerical electrons (*points*) having an energy greater than 40 keV at four different times: at $\omega_{pe}t = 5200$ (a), at $\omega_{pe}t = 5600$ (b), at $\omega_{pe}t = 8000$ (c) and at $\omega_{pe}t = 9000$ (d). The white plus designates the location of the maximum temperature in the system (118.7 MK).

and smaller spatial scales can be formed in the final state of fragmentation processes. Karlický et al. (2012) found that at the beginning of plasmoid merging processes, because of low values of the plasma β parameter in the initial state (as in coronal conditions), the fragmentation is caused by the magnetic tearing-mode instability. However, after a series of successive mergers of plasmoids, the plasma β parameter at some parts of the current sheet becomes greater than one. Then, not only the magnetic tearing-mode instability, but also the plasma flows start to be important. Thus, in the final state, the magnetic reconnection becomes turbulent like in the reconnection model of Lazarian and Vishniac (1999). However, this study, contrary to the model of Lazarian and Vishniac (1999), has shown how reconnection is changed from the initial state to the turbulent regime.

Distribution functions of the electrons, computed in this PIC simulation, were used for an evaluation of the hard X-ray emission and compared with that of the so called above-the-loop-top hard X-ray source observed by Krucker et al. (2010). Because the hard X-ray emission computed was similar to the observed one, the authors proposed that a sufficiently large plasmoid with a sufficient

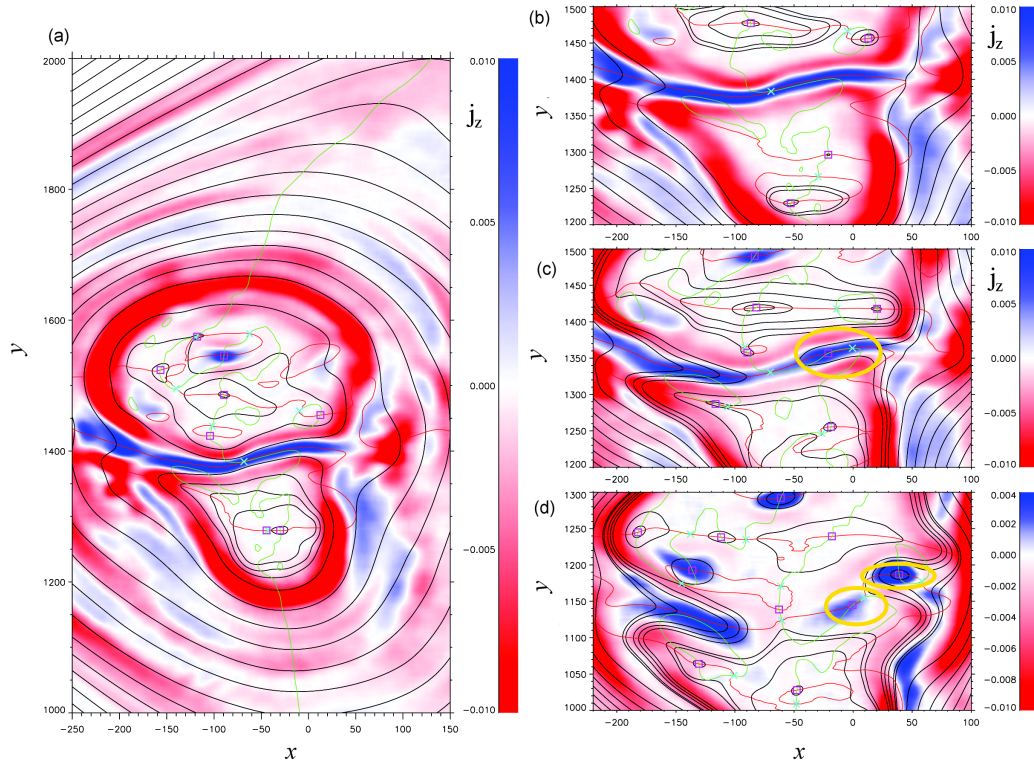


Fig. 5 Fragmentation of the current sheet (CS) between merging plasmoids. Figure displays the current density j_z -component (red-blue scale = negatively-positively oriented), magnetic field (black field lines), the lines of $B_x = 0$ and $B_y = 0$ (red and green lines, respectively), and the magnetic null points (X-points: cyan crosses, O-points: magenta squares). Panel (a) shows a larger view of the merging of two plasmoids at the time $t = 6000$. Panel (b) displays the situation at the same time but zoomed to the area around the positive CS formed between the merging plasmoids. Panel (c) shows the formation of the new X-O pair around $x = 0$, $y = 1350$ (marked by the gold ellipse) at the time $t = 6150$. Even further fragmentation in the already decaying CS between the plasmoids is seen at $t = 6700$ in panel (d) (gold ellipses).

amount of accelerated electrons trapped in this plasmoid can explain these above-the-loop-top hard X-ray sources.

3.3 Radio Emission from Merging Plasmoids

PIC codes enable us to compute acceleration processes, and they can also be used for studies of wave processes. In Figure 6 there are two boxes showing the magnetic field lines between two merging plasmoids. However, only one quarter of the plasmoid in each of the bottom corners of these boxes is presented. The packets of transverse (electromagnetic – radio) waves are displayed in the upper box, and the bottom box displays the packets of Langmuir (electrostatic) waves (black patches in the both boxes). This figure shows that Langmuir waves were generated inside the plasmoids due to instabilities of trapped accelerated electrons; compare this figure with Figure 4. On the other hand, the electromagnetic waves are generated at boundaries of the plasmoids, where they are converted

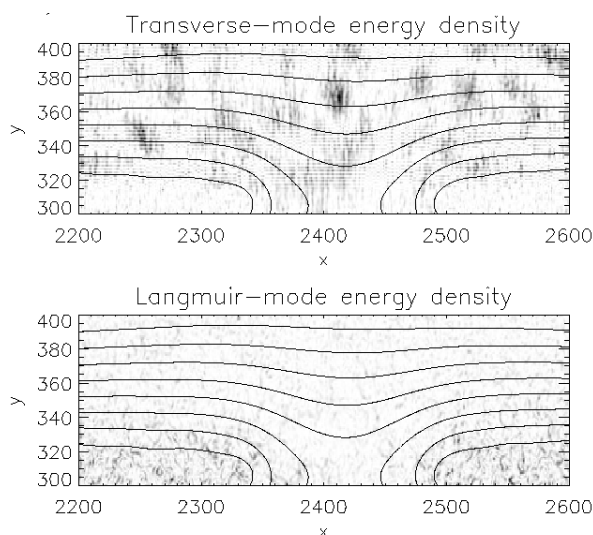


Fig. 6 PIC simulations: Transverse (electromagnetic) and Langmuir mode energy densities (*black patches*) at one instant during the merging of two plasmoids. Lines indicate the magnetic field lines.

from the Langmuir waves and escape out of the plasmoids. These electromagnetic waves are then observed by radiospectrographs. For further details, see Karlický et al. (2010). This simulation explains the generation of radio emission from the plasmoid; that is, the DPS and the narrowband dm-spikes. While the radio emission from the largest individual plasmoids corresponds to the DPSs, the same emission process, but from a cascade of many plasmoids with a power-law distribution in their sizes, produces a cloud of narrowband dm-spikes.

3.4 Cyclic Magnetic Reconnection

In solar flares, magnetic reconnection is considered to be a transient process in current sheets. However, in very hot plasma, when vortex plasma flows also become important, the cyclic type of magnetic reconnection can occur (Karlický 2009). To show this process, a 2.5-D electromagnetic PIC model was used. In the initial state, the model was a spatially homogeneous electron-proton plasma with the proton-electron mass ratio $m_p/m_e = 16$ and with the uniform magnetic field $\mathbf{B} \equiv (B_0, 0, 0)$, corresponding to the plasma beta parameter $\beta = 0.2$. The initial temperatures of electrons and protons were taken to be the same ($T_i = T_e$). To simulate a rotating plasma in the central part of the system, an external electric field E_z was added. For details, see Karlický (2009).

Figure 7 shows the time evolution of magnetic field lines in the plasma system during one rotation cycle of the plasma in its central part. As seen here, outside the rotating plasma the magnetic field lines become more and more stretched. The magnetic field lines show sudden changes in their orientation in the close vicinity of the rotating plasma, which indicates that there is an electric current in a thin layer around the whole rotating plasma. The amplification of the magnetic field as well as an increase in the stress of the magnetic field lines started in the upper-left and bottom-right quadrants of the system (Fig. 7(b)). On the other hand, in the upper-right and bottom-left quadrants the magnetic field lines form “V” structures, which later on evolve into X-type structures with oppositely oriented magnetic field lines (Fig. 7(c)). During magnetic reconnection at these locations (see the X-type structures at $x = 850 \Delta$, $y = 550 \Delta$, and at $x = 150 \Delta$, $y = 450 \Delta$ in Fig. 7(d)) the magnetic islands in the form of cuts of circles are produced. This process started at the boundary of the rotating

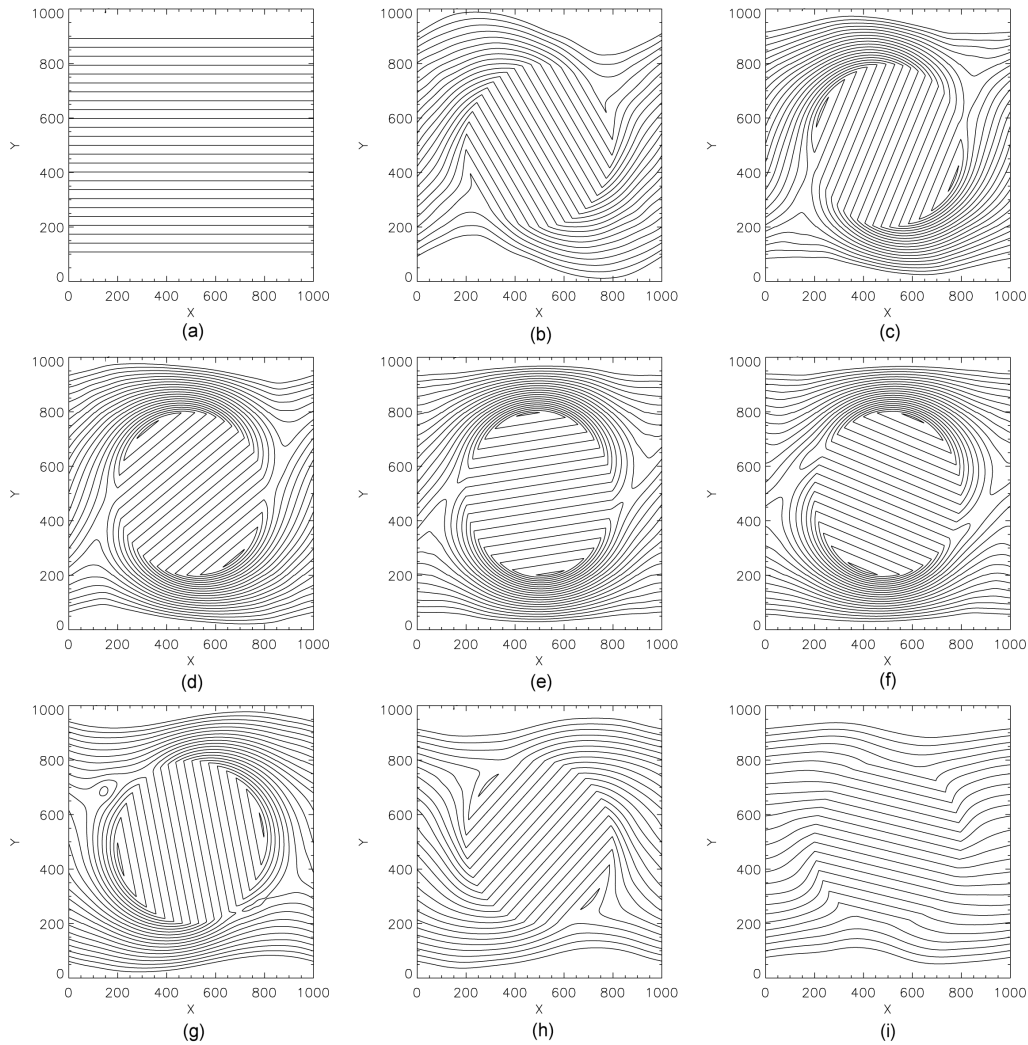


Fig. 7 PIC simulation: Magnetic field lines in the x - y computational plane at nine different times: at the initial state (a), at $\omega_{pe}t = 500$ (b), at $\omega_{pe}t = 1000$ (c), at $\omega_{pe}t = 1250$ (d), at $\omega_{pe}t = 1500$ (e), at $\omega_{pe}t = 1750$ (f), at $\omega_{pe}t = 2250$ (g), at $\omega_{pe}t = 2750$ (h) and at $\omega_{pe}t = 3250$ (i).

region and continued towards the center of rotation (Fig. 7(e)). It is finished when the orientation of the magnetic field lines in the rotating region is about opposite to that at the system boundaries (the lines $x = 0 \Delta$ and $x = 1000 \Delta$) (half of one rotation). Then, the role of the magnetic field reconnection changes: it opens the magnetic islands, the magnetic field stress decreases (Figs. 7(f)–(h)), and finally at the end of one full rotation, the structure of the magnetic field becomes similar to that at the initial state (compare Fig. 7(a) and Fig. 7(i)). This type of reconnection can appear around a rotating sunspot. Namely, a rotation of the sunspot increases the magnetic field energy around this sunspot. At these locations, the energy can be released by magnetic reconnection during a series of flares, see Vemareddy et al. (2012). On the other hand, this cyclic reconnection limits the amplification of the magnetic field in the dynamo process.

4 SIGNATURES OF MAGNETIC RECONNECTION PROCESSES IN SOLAR FLARES

4.1 Drifting Pulsation Structures

The most distinct signatures of plasmoids in dynamic radio spectra are the DPSs (Kliem et al. 2000; Karlický et al. 2001). Usually, DPSs are observed at the beginning of the impulsive phases of strong eruptive flares and then they drift towards lower frequencies, which corresponds to the upwards motion of the plasmoid. DPSs are associated with hard X-ray emission as well as with its hardening (Fig. 8 and Karlický et al. 2004). This indicates that the DPSs, and thus moving plasmoids, are associated with fast reconnection accelerating a huge amount of electrons. This behavior also agrees with the present model of magnetic reconnection. Namely, the motion of the plasmoid narrows the current sheet, where the reconnection is thus more effective.

In Figure 9, a very unique DPS with bi-directional features drifting to higher and lower frequencies is presented. Such drifting features indicate a separation of plasmoids in the stretching-tearing process somewhere in the central part of the reconnection (see the scheme of the fragmented reconnection in Fig. 10 (left)) (the details may be found in Jiříčka & Karlický 2011). Furthermore, in some cases, several DPSs are recorded, showing several plasmoids in the flare current sheets, see for example two positively drifting DPSs shown in Figure 10 (right). The positive drift of these DPSs means that the plasmoids move downwards in the flaring atmosphere.

4.2 Narrowband dm-spikes

Besides these DPSs, there are the so called narrowband dm-spikes (Benz 1986; Karlický 1984; Stähli & Magun 1986; Zlobec & Karlický 1998; Mészárosová et al. 2003; Kuijpers et al. 1981; Fleishman & Yastrebov 1994; Karlický et al. 2013), which were interpreted as generated in a cascade of plasmoids. As described in previous sections, many small plasmoids are generated between two merging plasmoids due to a fragmentation process. These plasmoids then interact and accelerate electrons, which produces plasma waves in each plasmoid, and thus generate a cloud of narrowband radio bursts – observed as dm-spikes, see for example Figure 10 (right). Searching for a characteristic bandwidth of individual spikes (Karlický et al. 1996; 2000) it was found that the Fourier spectrum of the dynamic spectra of spikes has a power-law form with power-law indices close to $-5/3$. Based on these results, it was proposed that the spikes are generated in turbulent reconnection outflows (Bárta & Karlický 2001). The global scenario of these processes is shown in Figure 10 (left). This scenario summarizes several aspects of the fragmentation of the flare current sheet. The plasmoids are formed due to a stretching of the current sheet by the rising main magnetic rope (see Fig. 1 (right)) and simultaneous tearing-mode instability. These plasmoids move and generate DPSs in the turbulent reconnection outflows of plasma. The plasmoids that move downwards are accumulated above the flare arcade, where they start to interact. During these interactions they are fragmented and generate a cascade of plasmoids and, thus, the narrowband dm-spikes. Compare this scenario with the DPSs and dm-spikes shown in Figure 10 (left) with those on the real radio spectrum (Fig. 10 (right)).

4.3 Plasmoids in X-ray Observations

The loop-top and the above-the-loop-top X-ray sources arise in the most discussed topics in recent years (Masuda et al. 1994; Tomczak 2001). Examples of such sources of soft X-rays can be found, for example in Milligan et al. (2010). An interesting example of the loop-top soft X-ray source that even merges with the downwards moving plasmoid is shown in Figure 11. This event was associated with the DPS.

Besides these soft X-ray sources, there are also those in hard X-rays, although they are very rare. Nevertheless, a very interesting example of the above-the-loop-top hard X-ray source was published by Krucker et al. (2010). They showed a source with energies up to ~ 80 keV which was located 6

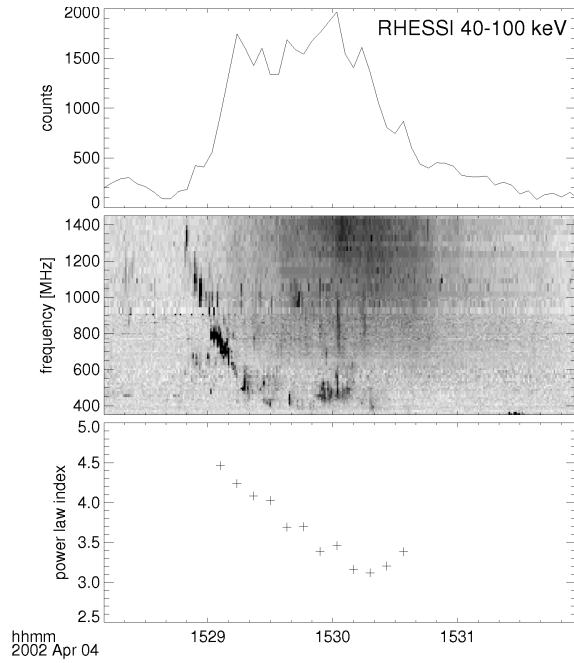


Fig. 8 Time evolution of the 2002 April 4 flare: RHESSI 40–100 keV counts (*top*), the 0.4–1.5 GHz radio spectrum showing the DPS observed by the Zürich radiospectrograph (*middle*), and the power-law index derived from RHESSI observations (*bottom*).

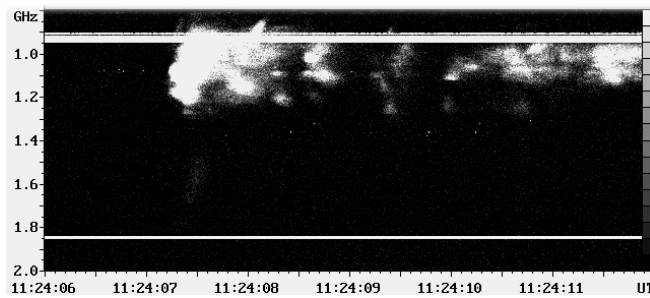


Fig. 9 The radio spectrum showing the pulsation structure with bi-directionally drifting features observed on 2010 February 12 by the Ondřejov radiospectrograph.

Mm above thermal flare loops. They derived the upper limit of the plasma density and source volume to be $n_e \sim 8 \times 10^9 \text{ cm}^{-3}$ and $V \sim 8 \times 10^{26} \text{ cm}^3$, respectively. They concluded that these hard X-ray sources have to be close to the acceleration region and the distribution function of electrons emitting hard X-rays is strongly non-thermal or the plasma in the source is very hot (up to $T_e \sim 200 \text{ MK}$).

As mentioned above, Karlický & Bárta (2011) calculated the X-ray spectra using the distribution functions computed in the PIC model of the successive merging of plasmoids in the vertical current sheet above the flare arcade. They showed that the observed emission from the above-the-loop-top

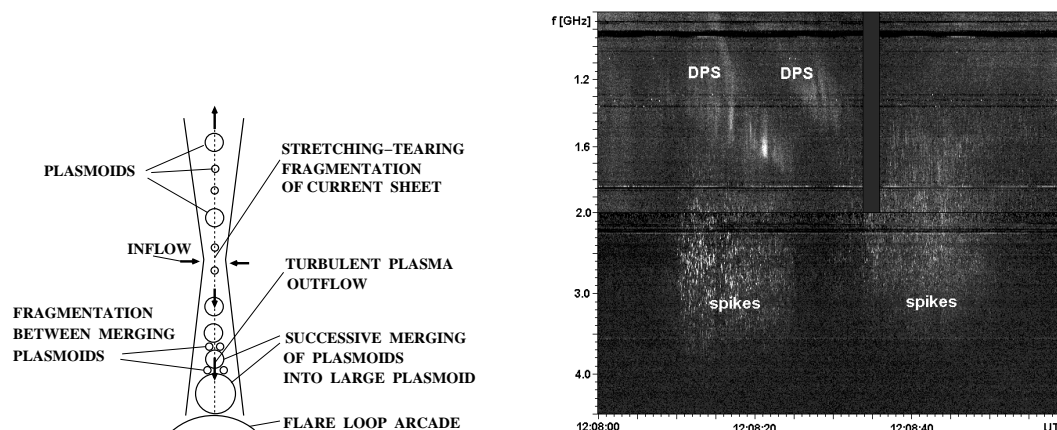


Fig. 10 *Left:* Scheme demonstrating the fragmentation of a current sheet. *Right:* The radio spectrum observed during the 2001 March 28 flare by two Ondřejov radiospectrographs (0.8–2.0 and 2.0–4.5 GHz). It shows the DPSs (radio signatures of large plasmoids) which drift towards narrowband dm-spikes (signatures of an interaction of fragmented plasmoids with the power-law distribution of their spatial scales); compare both parts.

hard X-ray source can be explained by the emission of superthermal and hot electrons (118.7 MK) trapped in a sufficiently large plasmoid.

4.4 Plasmoids in Kinked Magnetic Ropes

On 2001 April 18, the Nobeyama radioheliograph observed the C2.2 flare (in NOAA AR 9415) and its evolution is shown in Figure 12 (top). This flare exhibited a rising rope that was kinked due to its high twist and the kink instability. In this magnetic rope, several plasmoids were generated (see the arrows in this figure). They moved towards the top of the loop, where they merged into one compact plasmoid. Its brightness temperature and area then varied in antiphase, with a characteristic period of ~ 40 s. It was shown that these oscillations can be explained by a compression and rarefaction of this plasmoid. For details, see Karlický & Kliem (2010). This example shows that plasmoids can not only be formed in the current sheet below the rising magnetic rope (in the CSHKP flare model) (see Fig. 1), but also in the current sheets generated during a kinking of the magnetic rope (Kliem et al. 2010).

4.5 Mapping of Plasmoids into the Chromosphere

In magnetic reconnection, particles (electrons and ions) are accelerated in the region close to magnetic X-points (Zharkova et al. 2011). These particles propagate along magnetic field lines. The magnetic field lines, which connect the magnetic X-points in the low corona with the chromosphere, are generated by magnetic reconnection; these represent channels along which particles bombard the chromosphere and produce well known flare ribbons. Thus, processes in the magnetic reconnection are mapped on the chromosphere. In the standard flare model, a plasma together with magnetic field lines flows into one X-point of the vertical current sheet formed below a rising magnetic rope. Thus, the distance between two footpoints of the flare arcade (flare ribbons) increases, as observed in many flares. However, if in the vertical current sheet a plasmoid is moving downwards and interacting with the underlying arcade, then there are at least two X-points, which are mapped on the chromosphere.

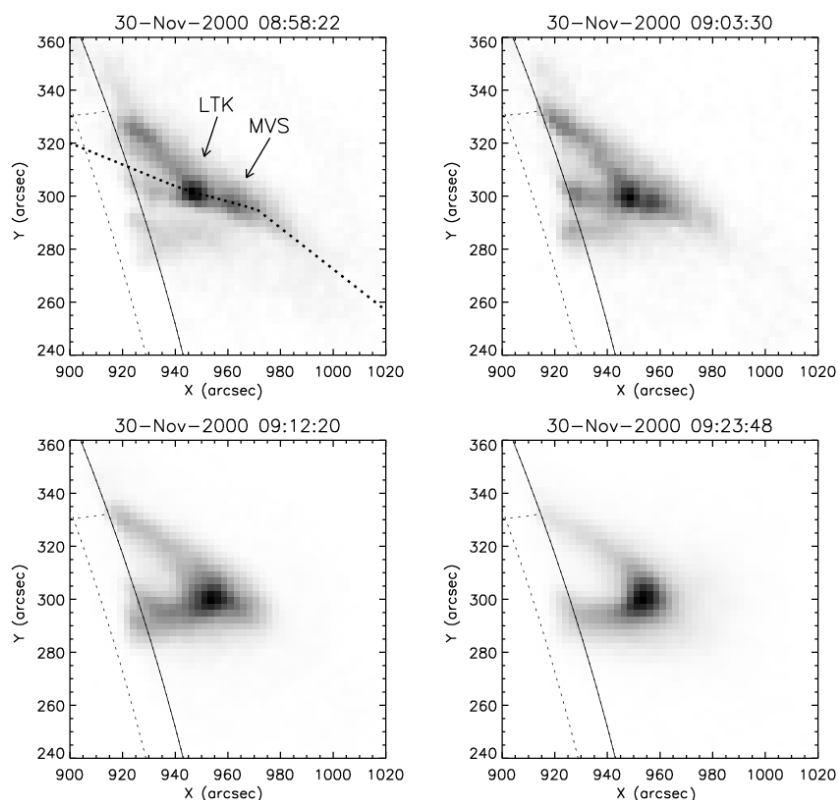


Fig. 11 Merging of downward moving plasmoid source (MVS) with the loop-top kernel (LTK) observed in X-rays by SXT/YOHKOH.

In this case, flare ribbons are split into two sub-ribbons (Fig. 2 second row top). Furthermore, during the interaction of the plasmoid with the flare arcade, the distance between ribbons can even decrease for a short time. For further details, see Bárta et al. (2011b). In real (three-dimensional) cases with more plasmoids, the form and behavior of flare ribbons can be very complex. Nevertheless, all these aspects give us a new view of flare ribbons.

4.6 Plasmoids in the White-light and Extreme-ultraviolet Emissions

Riley et al. (2007) presented the white-light observations of “rays” with moving blobs above the post eruptive flare loops. These “rays” were interpreted as current sheets. Because the thickness of these “rays” (about 1000 km) is much greater than that in any theoretically suggested current sheets (10–100 m), various possibilities explaining this difference have been discussed, see e.g. Lin et al. (2009).

Takasao et al. (2012) reported the SDO/AIA EUV observation of magnetic reconnection inflow and outflow in a flare on 2010 August 18. They found that during the flare’s impulsive phase, plasma blobs (plasmoids) appeared in the sheet structure above the flare arcade. The plasma blobs moved bi-directionally along the sheet structure (outflow); compare it with the bi-directional features in the DPS shown in Figure 9. This process was associated with the EUV threads moving toward the sheet structure (inflow). The upward and downward ejection velocities of the plasmoids were

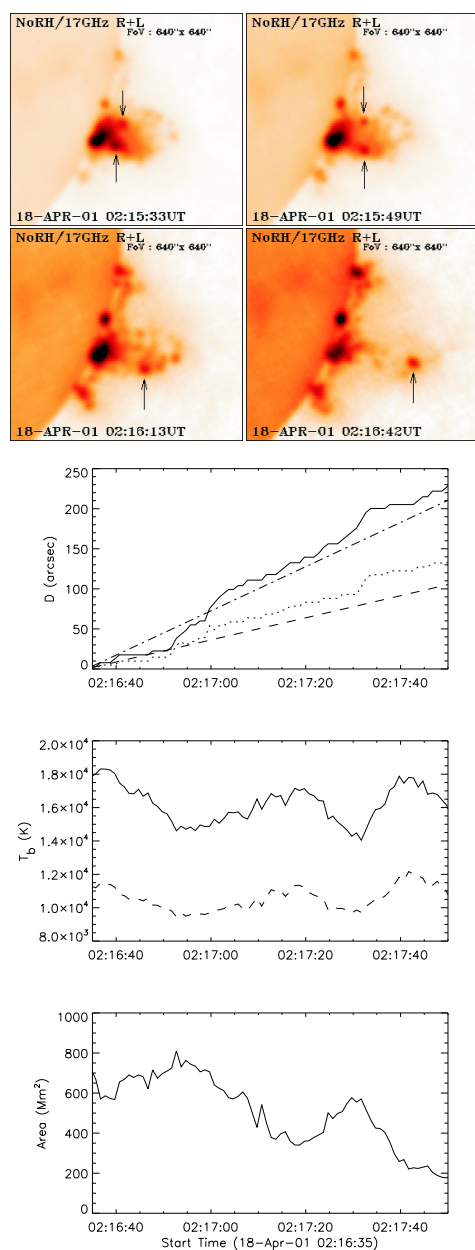


Fig. 12 *Top*: The 17 GHz Nobeyama radioheliograph images of the 2001 April 18 flare at four instants showing formation and ejection of the plasmoid (see arrows). *Bottom*: Time evolution of the parameters of the final plasmoid in the time interval of 02:16:35 – 02:17:50 UT; that is, after its formation. *Upper panel*: The distance of the plasmoid from its position at 02:16:35 UT along its trajectory (*solid line*). The dotted line expresses the distance of the plasmoid from its position at 02:16:35 UT in the east-west direction. The dashed and dash-dotted lines mean a change of the source position with a velocity of 1000 km s^{-1} and 2000 km s^{-1} , respectively. *Middle panel*: The maximum brightness temperature of the plasmoid (*solid line*) and the mean brightness temperature over the plasmoid area at half of the maximum brightness temperature (*dashed line*). *Bottom panel*: The plasmoid area at half of the maximum brightness temperature.

220–460 km s⁻¹ and 250–280 km s⁻¹, respectively. The inflow speed changed in the interval from 90 km s⁻¹ to 12 km s⁻¹. Furthermore, they found that some plasmoids in the sheet structure merged.

Similar observations were also presented by Savage et al. (2012). For a solar flare occurring on 2010 November 3, they showed the EUV observations of an erupting flux rope followed by inflows sweeping into a current sheet region. The inflows were soon followed by outflows appearing to originate from near the termination point of the inflowing motion; these agree with standard magnetic reconnection models. All these observations agree very well with the presented model of fragmented reconnection.

5 CONCLUSIONS

The present paper summarizes new results in studies of magnetic reconnection in solar flares. Very important processes, such as the fragmentation of the current sheet, formation of plasmoids and a cascade of plasmoids, are described. It was shown that fragmentation solves the problem of the thickness of the current sheet. Namely, at the very beginning of the flare the current sheet is relatively thick and needs to become very narrow with high current densities in some of its parts. Moreover, the fragmentation generates many X-points and, thus, there is enough plasma volume where the requested amount of particles are accelerated. Furthermore, it was shown that the processes that occur during plasmoid merging naturally lead to the turbulent regime of magnetic reconnection, in which magnetic instabilities (as in, for example, the tearing mode instability) and the plasma flows both play a role. This is due to strong heating during these processes and is, thus, due to an increase of the plasma β parameter.

We present examples of the DPSs, which are the most distinct radio signatures of plasmoids. It is proposed that the above-the-loop-top hard X-ray sources are large plasmoids with a sufficiently high plasma density and with a sufficient amount of energetic electrons trapped in this plasmoid. This model is in agreement with the conclusions made in the paper by Krucker et al. (2010), who found that the acceleration region is close to the above-the-loop-top hard X-ray source. The model can explain not only these hard X-ray sources, but also the loop-top sources. Considering all aspects of the associated fragmentation process (power-law spatial scales of plasmoids, effective acceleration of electrons, trapping of electrons in plasmoids, location in the reconnection plasma outflow) it was also proposed that these processes can explain the narrowband dm-spikes. This idea is supported by the statistical finding that more than 70% of all groups of narrowband dm-spikes are observed during the GOES-rising-flare phases (Jiříčka et al. 2001). However, the generation of the DPSs and narrowband dm-spikes is a very complex process that depends on many specific conditions. Thus, these bursts can only be observed in special cases. Furthermore, in some flares these bursts can be covered by strong radio continua or some continua can in reality be formed by a superposition of many narrowband dm-spikes. All these presented models can be supported by observations in the EUV and white-light ranges, where moving and interacting plasmoids together with plasma inflows and outflows were detected.

Magnetic reconnection is a universal process that plays an important role, not only in solar flares, but also in many other eruptive processes in the Universe, such as stellar flares, storms in magnetospheres of planets, even bursts in magnetars, and in processes associated with laboratory plasma experiments.

Let us finish this review by a short remark concerning plasma fusion devices such as Tokamaks (e.g. Rosenbluth 1994), which are expected to be a new source of energy. In these devices magnetic reconnection plays a negative role; together with various MHD instabilities it destroys the magnetic field structure of the plasma torus. Looking at the Tokamak system from the point of view of plasma processes in nature (solar flares and so on), this concept seems to oppose natural processes, especially the endeavor to generate a stable magnetic field structure in this system. It would be much more natural to utilize magnetic reconnection for plasma heating. Moreover, in the turbulent state

of reconnection, the magnetic field with a cascade of plasmoids (due to a fragmentation) will be so complex that it will effectively trap this very hot plasma. Furthermore, the concept of the cyclic reconnection (presented here) together with microwave heating can be used for additional plasma heating. Although I hope that the Tokamak system will be a successful source of energy, I think that the magnetic field reconnection in a dynamical equilibrium state should be considered in a more extended way in future fusion devices.

Acknowledgements This research was supported by grants P209/12/0103 (GA CR) and the Marie Curie PIRSES-GA-2011-295272 RadioSun project. M.K. thanks D. Nickeler for valuable comments.

References

- Aschwanden, M. J. 2002, *Space Sci. Rev.*, 101, 1
- Aurass, H., Mann, G., Zlobec, P., & Karlický, M. 2011, *ApJ*, 730, 57
- Bárta, M., & Karlický, M. 2000, *A&A*, 353, 757
- Bárta, M., & Karlický, M. 2001, *A&A*, 379, 1045
- Bárta, M., & Karlický, M. 2005, *ApJ*, 631, 612
- Bárta, M., Karlický, M., & Žemlička, R. 2008a, *Sol. Phys.*, 253, 173
- Bárta, M., Vršnak, B., & Karlický, M. 2008b, *A&A*, 477, 649
- Bárta, M., Büchner, J., & Karlický, M. 2010, *Advances in Space Research*, 45, 10
- Bárta, M., Büchner, J., Karlický, M., & Skála, J. 2011a, *ApJ*, 737, 24
- Bárta, M., Büchner, J., Karlický, M., & Kotrč, P. 2011b, *ApJ*, 730, 47
- Benz, A. O. 1986, *Sol. Phys.*, 104, 99
- Carmichael, H. 1964, in *AAS-NASA Symposium on Solar Flares*, ed. W. N. Hess (NASA SP-50), 451
- Drake, J. F., Shay, M. A., Thongthai, W., & Swisdak, M. 2005, *Physical Review Letters*, 94, 095001
- Drake, J. F., Swisdak, M., Che, H., & Shay, M. A. 2006, *Nature*, 443, 553
- Dryer, M., Andrews, M. D., Aurass, H., et al. 1998, *Sol. Phys.*, 181, 159
- Fleishman, G. D., & Yastrebov, S. G. 1994, *Sol. Phys.*, 154, 361
- Fletcher, L., Dennis, B. R., Hudson, H. S., et al. 2011, *Space Sci. Rev.*, 159, 19
- Fritzova-Svestkova L., Chase R.C., Svestka Z. 1976, *Sol. Phys.*, 48, 275
- Galsgaard, K., & Nordlund, Å. 1996, *J. Geophys. Res.*, 101, 13445
- Hirayama, T. 1974, *Sol. Phys.*, 34, 323
- Hoshino, M. 2005, *Journal of Geophysical Research (Space Physics)*, 110, A10215
- Hoshino, M., Nishida, A., Yamamoto, T., & Kokubun, S. 1994, *Geophys. Res. Lett.*, 21, 2935
- Jiříčka, K., Karlický, M., Mészáros, H., & Snížek, V. 2001, *A&A*, 375, 243
- Jiříčka, K., & Karlický, M. 2011, *Central European Astrophysical Bulletin*, 35, 215
- Karlicky, M. 1984, *Sol. Phys.*, 92, 329
- Karlicky, M., & Jungwirth, K. 1989, *Sol. Phys.*, 124, 319
- Karlický, M., Sobotka, M., & Jiříčka, K. 1996, *Sol. Phys.*, 168, 375
- Karlický, M., Jiříčka, K., & Sobotka, M. 2000, *Sol. Phys.*, 195, 165
- Karlický, M., Yan, Y., Fu, Q., et al. 2001, *A&A*, 369, 1104
- Karlický, M., Fárník, F., & Mészáros, H. 2002, *A&A*, 395, 677
- Karlický, M. 2004, *A&A*, 417, 325
- Karlický, M., Fárník, F., & Krucker, S. 2004, *A&A*, 419, 365
- Karlický, M., & Bárta, M. 2007, *A&A*, 464, 735
- Karlický, M. 2008, *ApJ*, 674, 1211
- Karlický, M. 2009, *ApJ*, 692, L72
- Karlický, M., Bárta, M., & Rybák, J. 2010, *A&A*, 514, A28
- Karlický, M., & Kliem, B. 2010, *Sol. Phys.*, 266, 71

- Karlický, M., & Bárta, M. 2011, *ApJ*, 733, 107
- Karlický, M., Bárta, M., & Nickeler, D. 2012, *A&A*, 541, A86
- Karlický, M., Bárta, M., & Jiříčka, K. 2013, *Central European Astrophysical Bulletin*, 37, 521
- Khan, J. I., Vilmer, N., Saint-Hilaire, P., & Benz, A. O. 2002, *A&A*, 388, 363
- Kliem, B., Karlický, M., & Benz, A. O. 2000, *A&A*, 360, 715
- Kliem, B., Linton, M. G., Török, T., & Karlický, M. 2010, *Sol. Phys.*, 266, 91
- Kołomański, S., & Karlický, M. 2007, *A&A*, 475, 685
- Kopp, R. A., & Pneuman, G. W. 1976, *Sol. Phys.*, 50, 85
- Krucker, S., Battaglia, M., Cargill, P. J., et al. 2008, *A&A Rev.*, 16, 155
- Krucker, S., Hudson, H. S., Glesener, L., et al. 2010, *ApJ*, 714, 1108
- Kuijpers, J., van der Post, P., & Slottje, C. 1981, *A&A*, 103, 331
- Kumar, P., Cho, K.-S., Chen, P. F., Bong, S.-C., & Park, S.-H. 2013, *Sol. Phys.*, 282, 523
- Kundu, M. R., Grechnev, V. V., White, S. M., et al. 2009, *Sol. Phys.*, 260, 135
- Lazarian, A., & Vishniac, E. T. 1999, *ApJ*, 517, 700
- Lin, J., Li, J., Ko, Y.-K., & Raymond, J. C. 2009, *ApJ*, 693, 1666
- Loureiro, N. F., Schekochihin, A. A., & Cowley, S. C. 2007, *Physics of Plasmas*, 14, 100703
- Masuda, S., Kosugi, T., Hara, H., Tsuneta, S., & Ogawara, Y. 1994, *Nature*, 371, 495
- Matsumoto, H., & Omura, Y. 1993, *Computer space plasma physics (Terra Sci. Publ. Comp, Tokyo)*, 74
- Meshalkina, N. S., Altyntsev, A. T., Zhdanov, D. A., et al. 2012, *Sol. Phys.*, 280, 537
- Mészárosová, H., Veronig, A., Zlobec, P., & Karlický, M. 2003, *A&A*, 407, 1115
- Milligan, R. O., McAteer, R. T. J., Dennis, B. R., & Young, C. A. 2010, *ApJ*, 713, 1292
- Nakariakov, V. M., Foullon, C., Verwichte, E., & Young, N. P. 2006, *A&A*, 452, 343
- Nickeler, D. H., & Wiegmann, T. 2012, *Annales Geophysicae*, 30, 545
- Nickeler, D. H., Karlický, M., Wiegmann, T., & Kraus, M. 2013, *A&A*, 556, A61
- Nisticò, G., Nakariakov, V. M., & Verwichte, E. 2013, *A&A*, 552, A57
- Norman, C. A., & Smith, R. A. 1978, *A&A*, 68, 145
- Odstrcil, D., & Karlický, M. 1997, *A&A*, 326, 1252
- Ohyama, M., & Shibata, K. 1998, *ApJ*, 499, 934
- Priest, E. R., & Forbes, T. G. 2002, *A&A Rev.*, 10, 313
- Pritchett, P. L. 2006, *Journal of Geophysical Research (Space Physics)*, 111, A10212
- Pritchett, P. L. 2008, *Physics of Plasmas*, 15, 102105
- Riley, P., Lionello, R., Mikić, Z., et al. 2007, *ApJ*, 655, 591
- Rosenbluth, M. N. 1994, *New Ideas in Tokamaks Confinement, Research Trends in Physics, American Institute of Physics, USA (Springer)*
- Savage, S. L., Holman, G., Reeves, K. K., et al. 2012, *ApJ*, 754, 13
- Schrijver, C. J. 2009, *Advances in Space Research*, 43, 739
- Shibata, K., & Tanuma, S. 2001, *Earth, Planets, and Space*, 53, 473
- Spicer, D. S. 1977, *Sol. Phys.*, 53, 305
- Staehli, M., & Magun, A. 1986, *Sol. Phys.*, 104, 117
- Sturrock, P. A. 1966, *Nature*, 211, 695
- Sych, R., Nakariakov, V. M., Karlický, M., & Anfinogentov, S. 2009, *A&A*, 505, 791
- Takasao, S., Asai, A., Isobe, H., & Shibata, K. 2012, *ApJ*, 745, L6
- Tan, B. 2013, *ApJ*, 773, 165
- Tanuma, S., Yokoyama, T., Kudoh, T., & Shibata, K. 2001, *ApJ*, 551, 312
- Thompson, B. J., Gurman, J. B., Neupert, W. M., et al. 1999, *ApJ*, 517, L151
- Tomeczak, M. 2001, *A&A*, 366, 294
- Ugai, M. 2013, *Journal of Atmospheric and Solar-Terrestrial Physics*, 99, 47
- Uzdensky, D. A., Loureiro, N. F., & Schekochihin, A. A. 2010, *Physical Review Letters*, 105, 235002

- Vemareddy, P., Ambastha, A., & Maurya, R. A. 2012, *ApJ*, 761, 60
- Vilmer, N., MacKinnon, A. L., & Hurford, G. J. 2011, *Space Sci. Rev.*, 159, 167
- Vlahos, L., Isliker, H., & Lepreti, F. 2004, *ApJ*, 608, 540
- Wang, X., & Yan, Y.-H. 2012, *RAA (Research in Astronomy and Astrophysics)*, 12, 1535
- Yan, Y., Huang, J., Chen, B., Liu, Y., & Tan, C. 2010, *Advances in Space Research*, 46, 413
- Zharkov, S., Green, L. M., Matthews, S. A., & Zharkova, V. V. 2013, *Sol. Phys.*, 284, 315
- Zharkova, V. V., Arzner, K., Benz, A. O., et al. 2011, *Space Sci. Rev.*, 159, 357
- Zlobec, P., & Karlický, M. 1998, *Sol. Phys.*, 182, 477
- Zuccarello, F., Contarino, L., Farnik, F., et al. 2011, *A&A*, 533, A100